Molecular Crystals and Liquid Crystals

Liquid Crystal Digital Beam Steering Device Based on Decoupled Birefringent Deflector and Polarization Rotator

Oleg Pishnyak [a] , Liubov Kreminska [a] , Oleg D.
Lavrentovich [a] , John J. Pouch [b] , Felix A. Miranda [b]
& Bruce K. Winker [c]

[a] Liquid Crystal Institute and Chemical Physics
Interdisciplinary Program, Kent State University,
Kent, Ohio

[b] NASA John H. Glenn Research Center, Cleveland,
Ohio

[c] Rockwell Scientific Company LLC, Camino Dos Rios,
Thousand Oaks, California

Version of record first published: 31 Aug 2006

PLEASE SCROLL DOWN FOR ARTICLE

Taylor & Francis
Taylor & Francis Group

Liquid Crystal Digital Beam Steering Device Based on Decoupled Birefringent Deflector and Polarization Rotator

Oleg Pishnyak
Liubov Kreminska
Oleg D. Lavrentovich
Liquid Crystal Institute and Chemical Physics Interdisciplinary
Program, Kent State University, Kent, Ohio

John J. Pouch
Felix A. Miranda
NASA John H. Glenn Research Center, Cleveland, Ohio

Bruce K. Winker
Rockwell Scientific Company LLC, Camino Dos Rios,
Thousand Oaks, California

We describe digital beam deflectors (DBDs) based on liquid crystals. Each stage of the device comprises polarization rotator and birefringent prism deflector. We used prisms made of the uniaxial smectic A (SmA) liquid crystal and a solid yttrium orthovanadate crystal. SmA prisms have high birefringence and can be constructed in a variety of shapes. We address the challenges of uniform alignment of SmA, such as elimination of focal conic domains. Rotation of linear polarization is achieved by electrically switched twisted nematic or electrically controlled birefringent cell. We describe a four-stage DBD steering a normally incident laser beam within ±56 mrad range with 8 mrad steps.

1. INTRODUCTION

Beam steering devices are in a great demand in space communication, optical fiber communications, optical switches, scanners [1–5], etc. In

279

addition to classical devices such as gimbals and mirrors, a number of other techniques is being under development nowadays, such as ceramic-based phase gratings [2], micro-electromechanical relief gratings [3], micromirror devices [4], decentered lens arrays, thermo-optic deflectors [5], photonic crystals [6–8] etc. Non-mechanical compact devices that are free of inertia problems are certainly the most sought-after. Liquid crystals are of special interest as active materials in non-mechanical beam steerers and deflectors, because of their structural flexibility, low operating voltage and low-cost fabrication [1,9]. Recent advances in synthesis of new LC materials [10] and in the design of the nematic LC cells [11] significantly improved parameters important for effective beam steering, such as optical birefringence and response times.

Among the prism-based DBDs, one of the most effective designs uses a cascade of elementary stages each of which represents a pair of an active polarization rotator and a prismatic deflector [12–19]. The advantage of such a decoupled design is that it allows one to separate the issue of the short response time (determined mostly by the switching speed of the rotator) and the angular range of deflection (determined by the geometry and optical properties of the deflector). Depending on the applied voltage, the active polarization rotator (LC cell) rotates the polarization of incident light by $\pi/2$ or leaves the polarization intact. A passive birefringent prism separates the beam into two channels, depending on the beam polarization. The decoupled pair of a rotator and deflector has no moving parts and can be cascaded into N stages, making 2^N addressable beam directions.

The liquid crystals can be used in both active and passive elements of prism-based DBD, as they demonstrate a relatively high optical birefringence (in the range 0.1–0.4) and relatively fast switching speed (milliseconds), see, for example, Ref. [11]. Application of LCs for polarization switching is a well-developed field, mostly because the TN and similar nematic cells are at the heart of modern LC display devices [20].

In this article we describe a four-stage DBD switched by four TN or ECB cells. The TN cells are coupled to the passive solid crystal (yttrium orthovanadate) prisms. The DBD switches optical beam at 633 nm in the range ±56 mrad with 8 mrad steps. Application of LCs in the passive prismatic elements is less studied, despite their apparent advantages, such as structural flexibility and low-cost fabrication. One of the reasons for such a neglect is that a LC-based prism with a substantial dihedral angle α (needed for the substantial angle of beam deflection) and a substantial aperture A should be relatively thick, up to $h = A \tan \alpha$. If h is in the range of millimeters and centimeters, then

huge losses caused by light scattering at director fluctuations [21,22] rule out the applicability of the nematic LCs. In this article we describe passive prismatic element formed by a uniaxial SmA LC and by solid crystals. The advantage of the SmA materials over nematic LCs is that director fluctuations are suppressed by the layered smectic structure.

2. BIREFRINGENT MATERIALS

2.1. SmA LC materials

In SmA, the elongated rod-like molecules are arranged in a periodic stack of layers with the director **n** (a unit vector that shows the average local direction of molecules and thus the optic axis of the material) being perpendicular to the layers; the states **n** and $-$**n** are identical. Inside the layer the molecular centers of gravity show no long-range order, thus each layer is a two-dimensional fluid. Positional order along **n** significantly reduces thermal director fluctuations and thus reduces light scattering [21,22]. However, the very same layered structure brings about another possible source of scattering, namely, static director distortions such as undulations and focal conic domains (FCDs) [23].

Usually, the LCs are aligned by an appropriate treatment of the bounding plates of the cell (e.g., buffing of a thin polyimide layer). In flat nematic cells such an alignment is often sufficient to achieve a monodomain state. In SmA, however, even perfect surface alignment does not exclude undulations and FCDs as they can be caused by the mechanical response of the cell to varying temperature or by a small foreign particle in the bulk. To eliminate undulations and FCD in SmA, one might use a strong magnetic or electric field. However, as shown by Luckhurst *et al.*, SmA samples are still hard to align as monodomains [24,25]. Below we quantify the process of field alignment of SmA, by considering the behavior of a FCD in an applied magnetic field [23].

FCD can be stabilized by a mechanical impurity in the bulk or at the surface of the cell, or emerge as the result of the preceding undulation (periodic tilt and dilation) of SmA layers [23]. These undulations can be caused by shrinkage of the SmA layers when the material is cooled down (cooling is needed as the cell filling is facilitated at high temperatures when the viscosity is low). As molecular layers in many SmA materials, such as cyanobiphenyls, are composed by pairs of oppositely oriented polar molecules, their thickness can vary significantly, from the value close to the length of one molecule to about
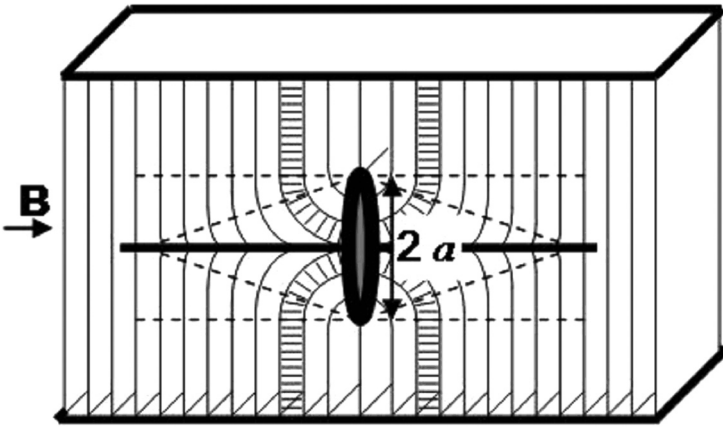
FIGURE 1 Schematic view of toric FCD. The SmA layers are perpendicular to the substrates and folding within the FCD. The director changes the orientation on $90°$ from tangential outside the FCD to vertical within the FCD to satisfy the boundary conditions at the disk-like foreign particle in the SmA bulk.

twice of this value. These polar materials are especially hard to align [26]. Non-polar SmA show one-molecule layers with thickness that is not so strongly affected by temperature.

The known description of undulations [20,21] refers to the case when the molecules are aligned perpendicularly to the bounding plates (homeotropic alignment). In our case, however, the plates set planar orientation with the molecules aligned parallel to the plates and to the dihedral edge of the prism, Figure 1. One can obtain a close estimate of the magnetic field needed to align the SmA uniformly, by considering the behavior of the FCDs, as the FCDs are the most developed departures from the uniform alignment of SmA. We consider the simplest type of FCD, the so-called toric FCD that can be stabilized by a foreign particle in the SmA bulk [27,28] (Fig. 1).

The toric FCD is based on a pair of linear defects, a circular defect line and the straight line passing through the center. The smectic layers are wrapped around the pair as shown in Figure 1. Note that outside the FCD the molecules are oriented uniformly along a single axis parallel to the plates.

Suppose a small toric FCD with the radius a of the defect circle much smaller than the lateral size of the cell, is stabilized in an otherwise uniform SmA sample by a particle, which sets tangential orientation of SmA molecules at its surface. For the sake of simplicity,

we approximate the particle by a disk of radius R and zero thickness (Fig. 1). If the SmA were uniform, the director would be in an unfavorable perpendicular orientation at the plate. The FCD would be stable if its elastic energy [29]

$$F_{el} = 2\pi^2 aK[\ln(2a/r_c) - 2 - \bar{K}/K] + F_c, \tag{1}$$

(where K is the splay elastic constant, $\bar{K}$ is the saddle-splay constant, r_c is the core radius of the circular defect, and F_c is the core energy of the circle and the straight line) is smaller than the anchoring energy difference between the FCD-free (uniform) state and the FCD state:

$$\Delta F_s = 2\pi a^2 W, \tag{2}$$

where W is the surface anchoring coefficient for director deviations in the plane normal to the particle's surface, the so-called polar anchoring coefficient. In SmA, $W \sim (10^{-3} - 10^{-2})\,\mathrm{J/m^2}$ is orders of magnitude higher than the corresponding value in the nematic phase, where typically $W \sim (10^{-5} - 10^{-4})\,\mathrm{J/m^2}$ [30].

If the anisotropy $\chi_a = \chi_\parallel - \chi_\perp > 0$ of SmA diamagnetic susceptibility is positive, then applying the field in the direction of the desired orientation of molecules should reduce the FCD, as the molecules inside the domain should reorient along **B**, Figure 1. The diamagnetic energy gain from such a reorientation is $\Delta F_B = \int \frac{1}{2}\mu_0^{-1}\chi_a B^2 \sin^2\theta\,dV$, where $\mu_0 = 4\pi \times 10^{-7}\,\mathrm{N/A^2}$ is the permeability of free space, θ is the angle between the director and **B**, the volume element is $dV = r(a - r/\sin\theta)\sin\theta\,d\theta\,d\varphi\,dr$; r and $r - a/\sin\theta$ are the principal radii of curvature of SmA layers within the toric FCD, r varies in the range from 0 to $a/\sin\theta$; $0 \le \Theta \le \pi$; $0 \le \varphi < 2\pi$. Integration yields

$$\Delta F_B = \frac{1}{3}\mu_0^{-1}\chi_a B^2 a^3, \tag{3}$$

The stability of the FCD is determined by the energy difference between the FCD state and the uniform state, comprised of the elastic, surface anchoring, and diamagnetic contributions, $\Delta F = \Delta F_s - F_{el} - \Delta F_B$:

$$\Delta F_B = 2\pi a^2 W - 2\pi^2 aK\left[\ln\frac{2a}{r_c} - 2 - \frac{\bar{K}}{K}\right] - F_c - \frac{1}{3}\mu_0^{-1}\chi_a B^2 a^3 \tag{4}$$

Figure 2 shows the function $\Delta F(B)$ for two different sizes of FCDs, of radius $a = 1\,\mu\mathrm{m}$ and $0.4\,\mu\mathrm{m}$, calculated for the following typical values of parameters: $K = 10^{-11}\,\mathrm{N}$, $\bar{K} = 0$, $W = 10^{-2}\,\mathrm{J/m^2}$, $r_c = 10\,\mathrm{nm}$, $F_c = 0$ (r_c is chosen to adsorb the core energy into the elastic energy of layer distortions [24]), and $\chi_a = 10^{-5}$ [30]. The plot clearly
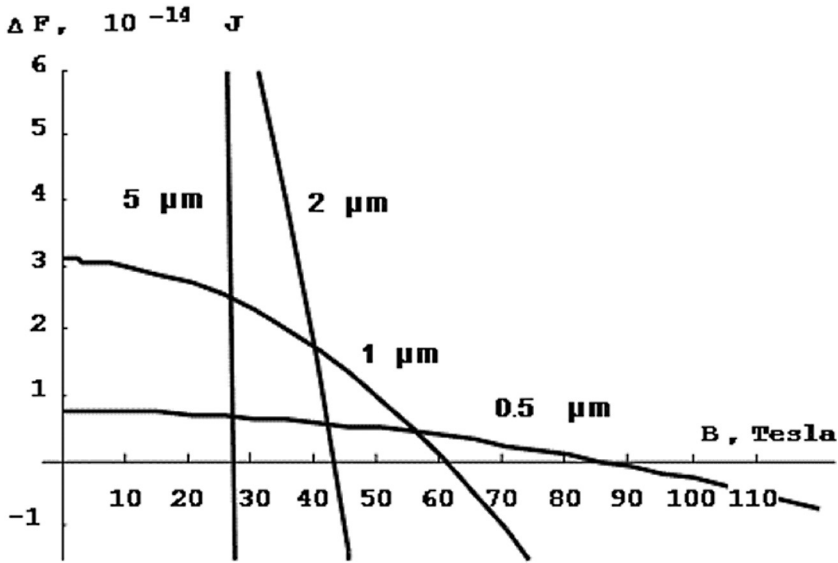
FIGURE 2 Free energy difference between the uniform state of a SmA slab with an incorporated foreign particle-disk and the state with the toric FCD, as the function of the magnetic field applied to align the director uniformly.

demonstrates that to reduce the size of FCD to sub-wavelength (in visible and near-IR) scale, one would need huge magnetic fields of the order of tens and hundreds of Tesla.

Now let us compare this estimate to the magnetic field needed to realign the director around a foreign particle in the nematic phase, where the polar anchoring is usually much weaker. The magnetic field would be able to realign the director around a foreign particle completely when the corresponding diamagnetic coherence length $\xi = \frac{1}{B}\sqrt{\mu_0 K/\chi_a}$ is smaller than the anchoring extrapolation length $l = K/W$, i.e., when the magnetic field is larger than

$$B_c = W\sqrt{\frac{\mu_0}{K\chi_a}}. \tag{5}$$

Therefore, $B \sim 1\,\mathrm{T}$ would be sufficient to suppress the director distortions around a particle with $W \sim 10^{-5}\,\mathrm{J/m^2}$; $B \sim 10\,\mathrm{T}$ would be needed if $W \sim 10^{-4}\mathrm{J/m^2}$, etc. Therefore, magnetic alignment is much easier in the nematic phase than in the SmA phase.

Consideration above suggests that in order to minimize the light losses, one should search for the SmA material composed of nonpolar

(a)
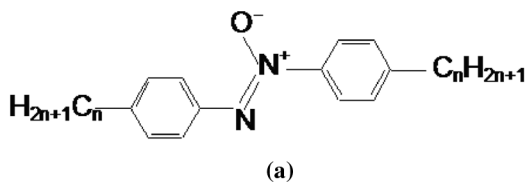
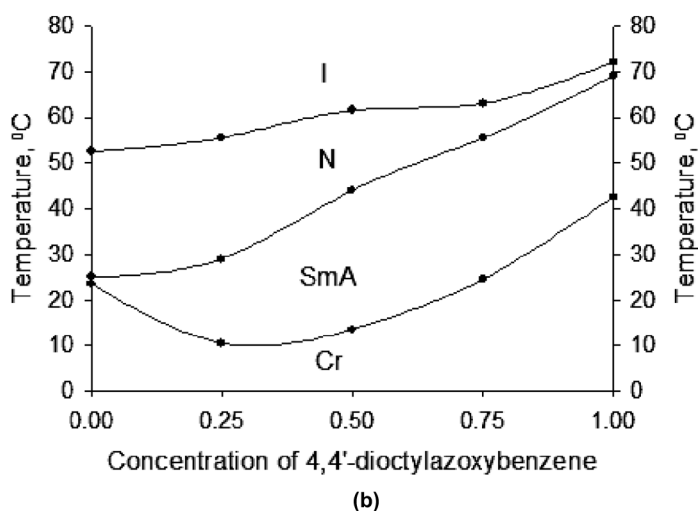Phase diagram of 4,4'-dihexylazoxybenzene and 4,4'-dioctylazoxybenzene mixture

(b)

FIGURE 3 Molecular structure of 4,4′-*n*-dialkylazoxybenzene (a); Phase diagram of the binary mixture of n = 6 and n = 8 homologues of 4,4′-*n*-dialkyl-azoxybenzene (b).

molecules, which has not only a SmA but also a nematic phase. The material can be aligned in the nematic phase and then slowly cooled down to the SmA phase to obtain a low-scattering birefringent sample.

The requirements above are met by low-molecular weight 4,4′-*n*-dialkylazoxybenzenes as demonstrated first in Ref. [12,13], Figure 3a. We developed these materials further and used n = 5, 6, 7, 8 homologues of 4,4′-*n*-dialkylazoxybenzene purchased from Sigma-Aldrich Chem. Co to prepare mixtures with a broad temperature range of SmA phase. All the LC components were purified to decrease the contents of undesired dopants and foreign particles. The temperature range of SmA phase can be expanded to about 30 degrees in eutectic mixtures. The mixture of n = 6 and n = 8 homologues in proportion 1:1 shows the best deflection efficiency (a ratio

of intensities of the deflected and incident beams) and a good thermal range (Fig. 3b). These mixtures were used as a SmA filler for passive prismatic deflectors.

3. OPTICAL ELEMENTS: PRISMS AND POLARIZATION ROTATORS

In this section we describe properties and performance of optical elements used in single-stage beam-deflection schemes, namely, the SmA and solid YVO$_4$ prisms, and rotators of polarization based on TN and ECB cells.

3.1. Single SmA prisms

The prismatic cell filled with LC material has following geometry: two glass plates with rubbed polyimide layers (PI2555, Microsystems) formed a wedge cell, which was filled with the SmA blend of 4,4′-dihexylazoxybenzene and 4,4′-dioctylazoxybenzene in proportion 1:1. The assembled cell was heated to the isotropic state and slowly cooled down to the room temperature with the temperature rate $\sim 5 \times 10^{-4}$ K/s in 1.2 Tesla magnetic field. The measured parameters of the birefringent prism are as following:

- wedge angle: $15.8°$;
- refractive indices of the SmA mixture (at $\lambda = 633$ nm and temperature $22°$C): $n_e = 1.72$, $n_o = 1.53$, $\Delta n = 0.19$;
- steering angles: for the light polarized parallel to the LC director (extraordinary wave) $\theta = 12.2°$, for the light polarized perpendicular to the LC director (ordinary wave) $\theta = 8.9°$;
- efficiency of the deflected beams (the ratio of the deflected beam intensity to the intensity of incident beam) for 0.5 cm aperture of the incident beam at the cell thickness 500 microns: for the light polarized parallel to the LC director (extraordinary wave) 85%, for the light polarized perpendicular to the LC director (ordinary wave) 88%.

SmA-filled elements have obvious advantages in comparison with solid crystalline prisms. First of all, SmA prisms are easier to prepare, as they do not require polishing and fine controlling of the optical axis during manufacturing, which is very critical in the case of crystalline prisms. The optical axis of SmA prisms can be easily set by the rubbing direction of the aligning polyimide or/and direction of the applied external field. SmA materials allow one to construct low-cost

wide-aperture birefringent elements in different geometries including various prisms, arrays of microprisms etc.

Among the disadvantages of SmA-filled elements is light scattering at the residual FCDs, which remain after aligning process. The alignment of SmA material is sensitive to the abrupt temperature fluctuations as well. The SmA prisms can only operate within the temperature range of the SmA phase; drastic temperature changes might cause a complete misalignment of the material.

3.2. Crystalline Birefringent Biprisms

SmA liquid crystals might serve as good materials to construct inexpensive, large-aperture birefringent elements such as prismatic deflectors. The advantages of SmA are especially evident when complex geometries are needed, e.g., prisms with curved surfaces. However, SmA are still hard to align and when high-quality optical performance is required, regular solid crystal prisms might be preferable.

We have chosen solid crystal yttrium orthovanadate YVO$_4$ as the high-optical quality material for the passive beam deflectors. YVO$_4$ is an optically positive uniaxial crystal of a tetragonal structure with a large birefringence ($n_o = 1.9929$, $n_e = 2.2154$, and $\Delta n = n_e - n_o = 0.2225$ at $\lambda = 633$ nm), a wide transparency range (400–5000 nm) and good temperature stability.

We used Rochon biprisms [31] (RPs) made of the solid crystalline YVO$_4$ as passive birefringent discriminators in the assembled DBD. RP is composed of two prisms at wedge angle α and cemented together. Optical axes of two prisms are perpendicular to each other. A beam with the E-vector oscillating perpendicularly to optic axis in both parts of the RP (p-wave) is an ordinary wave and it is transmitted without deflection. The beam with the E-vector oscillating perpendicularly to the optic axis of first part and parallel to the optic axis of the second part of RP (s-wave) becomes an extraordinary wave in the second prism. To the approximation of small angles the deflection angle Θ^{out} depends on the optical birefringence Δn, wedge angle α of the RP, and an incident angle Θ_s^{in},

$$\Theta_s^{out} = \Delta n \alpha + \Theta_s^{in} \tag{6}$$

The wedge angle α of the RP that would change the angular direction of propagation from an incident angle Θ^{in} into a desirable angle Θ^{out} is calculated as

$$\alpha = (\Theta_s^{out} - \Theta_s^{in})/\Delta n. \tag{7}$$

3.3. Fast Polarization Rotators

Both ECB and 90° TN cells represent good candidates for electrically-controlled polarization switchers because technology is well established.

The TN cell [32] is assembled from two glass plates with tangential director alignment along two mutually perpendicular axes at the opposite plates and filled with a slightly chiral nematic LC. Depending on the applied voltage, the TN cell can be in either the "OFF" state, with the emerging light polarization of linearly polarized beam rotated by 90° ($\pi/2$- wave) or the "ON" state, with the same light polarization (0-wave), (Fig. 4a).

We achieved a transmission coefficient of 94% for the $\pi/2$-wave and 97% for the 0-wave by using TN cells with antireflection coatings. The coefficient is determined as the ratio of the output beam intensity to the incident beam intensity. The light leakage of undesirable orthogonal polarization was less than 0.5%.
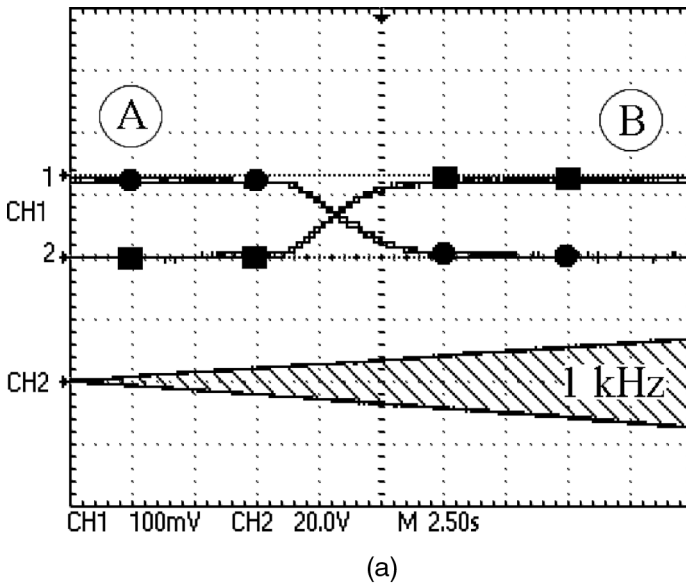

(a)

FIGURE 4 Oscillograms of the TN cell (a) transmission (curve 1 marked by dots: crossed polarizer and analyzer and curve 2 marked by squares: parallel polarizer and analyzer) vs applied voltage; and ECB cell, applied voltage increased from 0 to 10 V at 1 kHz; at 50 kHz transmission was the same as at 0 V (b) (curve 1: crossed polarizer and analyzer), applied voltage decreased from 10 to 0 V at 50 kHz and then increased from 0 to 10 V at 1 kHz.
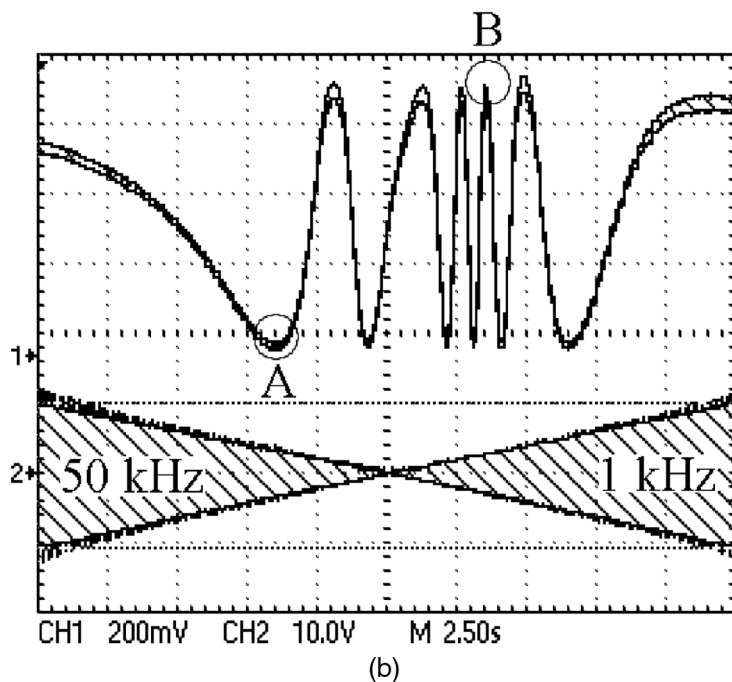
FIGURE 4 Continued.

Nematic cells (with electrically controlled birefringence (ECB)) were assembled in an antiparallel fashion from glass plates coated with conducting indium tin oxide and obliquely deposited thin SiO layers, which yield a high pretilt angle of 45° that the director makes with the substrate. Electric voltage applied to the ITO aligns the director perpendicularly to the plates (homeotropic state) when $f < f_c$ (1 kHz, Fig. 4b), and parallel to the plates when $f < f_c$ (50 kHz).

Both ECB and TN cells were filled with the dual frequency nematic MLC-2048 material (purchased from EM Industries). MCL-2048 has a large birefringence $\Delta n = 0.221$ and can be switched very quickly, within tenths of a millisecond in relatively thick cells.

The typical transmission-voltage curves for normal light incidence are shown in Figure 4a, b for TN and ECB cells respectively.

Use of special short pulses of applied voltage of low and high frequency lead to fast switching between A ⇔ B states on the order of ms or less [11].

4. DESIGN OF THE DBD

4.1. Modeling

We designed a DBD composed of four stages that deflects an incident He-Ne laser beam into $2^4 = 16$ directions within the range ± 56 mrad with 8 mrad steps (Fig. 5). Each stage is composed of a LC cell as the polarization rotator and a solid crystal YVO_4 Rochon prism as the passive deflector. The maximum deflection angle increases by a factor of 2 from the first stage to the third stage. The fourth prism deflects into the opposite angular direction, as it is flipped with respect to all other prisms, as shown in Figure 5.

Table 1 shows the calculated wedge angles α of YVO_4 prisms that provide the required angular deviations $\Theta^{in} \to \Theta^{out}$ at $\lambda = 633$ nm, see Eq. (7). The four prisms with wedge angles specified in Table 1 were custom made by Conex Systems, Inc. and coated with the anti-reflective film by Thin Film Technology, Inc.

To illustrate the sequence of deflections, let us trace the normally incident laser beam transmitted through the proposed DBD.

(1) After first LC cell the wave has s-polarization. The first prism (RP1) increases the deflection angle the wave from 0 mrad to $+8$ mrad. The second prism (RP2) deflects the s-wave to $+24$ mrad. The third prism RP3 enlarges the angle to $+56$ mrad. The fourth LC cell changes the state of s-polarization into p-polarization. The p-wave passes the 4th prism (RP4) unaltered at $+56$ mrad.
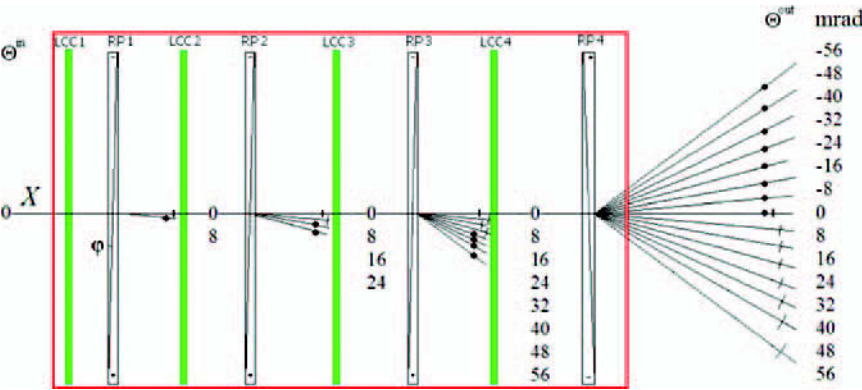

FIGURE 5 Sketch of the DBD device. Black bars and dots mark the direction of the optic axis of the RP. Angles are measured in mrad. For the sake of simplicity, wave normals start from the center of each optic element.

TABLE 1 RPs: The Wedge Angle α and Deflection of an Incident s-wave $\Theta^{in} \to \Theta^{out}$

	RP1	RP2	RP3	RP4
$\Theta^{in} \to \Theta^{out}$, mrad	$0 \to 8$	$8 \to 24$	$32 \to 64$	$8 \to 64$
α, deg	$2.06°$	$4.12°$	$8.20°$	$14.17°$

(2) The p-wave after first LC cell passes through the first three prisms without changing the input angle of 0 mrad. The fourth LC cell changes the state of p-polarization into s-polarization. The 4th prism (RP4) deviates this s-wave to -56 mrad.

As just demonstrated, the DBD deflects the normally incident laser beam into the range $(-56 \text{ mrad}, +56 \text{ mrad})$. A small non-zero incident angle Θ^{in} change the range of deflection angles approximately as $(-56 \text{ mrad} + \Theta^{in}, +56 \text{ mrad} + \Theta^{in})$.

4.2. Experimental Setup

We assembled the DBD from four pairs of RP and TN as shown in Figure 5. All optical elements were placed on adjustable Newport Gimbal Optical Mounts. The He-Ne laser with the polarization ratio 200:1 was used as the source of linearly polarized coherent light at $\lambda = 633$ nm. The multi-channel Waveform Generator WFG 500 (FLC Electronics) was automated by LabView software to address the TN cells. We measured the light intensity by the Newport Optical Power Meter Model 835.
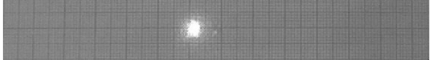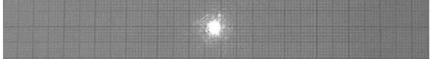
The pattern of steered beams was captured by the CCD-camera in the focal plane of the focusing convergent lens with the focal length f = 1 m. We measured the output deviation angle in the focal plane of the lens as ArcTan(Δ/f), where Δ is the beam displacement. Each displacement by 1 mm corresponds to 1 mrad angle.

5. EXPERIMENTAL RESULTS AND DISCUSSION

The DBD deviated the normally incident laser light into the range $(-56 \text{ mrad}, +56 \text{ mrad})$ with the step of 8 mrad as shown in Table 2. The addressing of TN cells was performed accordingly to the algorithm of Table 2. All deflection states are independent of each other.

Table 2 shows how four TN cells control the deflection of a p-wave, as an example. The symbols "0" and "$\pi/2$" means "polarization unchanged" and "polarization rotated by $\pi/2$". The number NN marks

O. Pishnyak et al.

TABLE 2 Sequence of Patterns of Laser Beams Steered by the DBD. Beams are Displaced on 8 mm that Corresponds to the 8 mrad Angle. All Elements of the DBD had Antireflection Coating

NN	Θ, mrad	Pattern	TN cells operation mode			
			TN1	TN2	TN3	TN4
1	-56		0	0	0	$\pi/2$
2	-48		$\pi/2$	$\pi/2$	0	$\pi/2$
3	-40		0	$\pi/2$	$\pi/2$	$\pi/2$
4	-32		$\pi/2$	0	$\pi/2$	$\pi/2$
5	-24		0	0	$\pi/2$	0
6	-16		$\pi/2$	$\pi/2$	$\pi/2$	0
7	-8		0	$\pi/2$	0	0
8	0		$\pi/2$	0	0	0
9	0		0	0	0	0
10	8		$\pi/2$	$\pi/2$	0	0
11	16		0	$\pi/2$	$\pi/2$	0
12	24		$\pi/2$	0	$\pi/2$	0
13	32		0	0	$\pi/2$	$\pi/2$
14	40		$\pi/2$	$\pi/2$	$\pi/2$	$\pi/2$
15	48		0	$\pi/2$	0	$\pi/2$
16	56		$\pi/2$	0	0	$\pi/2$

the mode of operation of the whole set of TNs. For example, for the line NN = 9 in Table 2, which corresponds to the "0000" mode, all four TN cells transmit the input light without change of the polarization, the total deflection angle is 0 mrad. Switching of 4th TN to the rotation

mode, "$000\pi/2$", results in the deflection angle $\Theta^{out} = -56$ mrad (line $NN = 1$) and so on. There are sixteen deflected directions (direction "0 mrad" appears twice for p- and s-waves, NN 8,9). A slight mutual displacement of patterns NN8 and NN9 is caused by the finite manufacturing tolerance (1 mrad) of the fourth RP.

The light transmission of the DBD is strongly reduced by reflection losses at the crystal/air and glass/air interfaces because refractive indices of the used materials are different: $n_{glass} = 1.5$ for the glass, $n_o = 1.4978$, $n_e = 1.7192$ for the liquid crystal MLC-2048, and $n_o = 1.9929$, $n_e = 2.2154$ for YVO$_4$. To increase the transmission of the DBD, we constructed and tested the performance of DBD in which the surfaces of RPs and TN cells in contact with air were coated with antireflective films designed for $\lambda = 633$ nm. The resulting light transmission through the four-stage DBD increased to 75%. The intensity of the brightest parasitic beam caused by reflection at the interfaces was less than 1.6% of the intensity of incident light.

6. CONCLUSIONS

We demonstrated the principle of non-mechanical digital beam deflection based on decoupled pairs of electrically-controlled liquid crystalline polarization switchers such as TN cells and passive deflectors, such as SmA or crystalline birefringent prisms. The scheme allows one to separate the issue of time response and beam deflection angles and optimize these two parameters separately. For example, one can replace the TN cells with electrically-controlled birefringent cells based on dual-frequency nematic liquid crystals and achieve submillisecond response times [11].

The deflection angles can be optimized by the design of the birefringent prisms. Smectic A-filled prisms are attractive in low-cost applications where one needs large apertures, large angles of deflection, and/or non-trivial geometries. We demonstrated that mixtures of homologues of 4,4′-n-dialkylazoxybenzene produce SmA phases with a broad temperature range of SmA existence (up to 30 degrees C for binary mixtures) with a relatively small number of residual defects such as focal conic domains. We demonstrated that typical magnetic fields needed to align the director field uniformly in the SmA phase is one-two orders of magnitude higher than the corresponding field needed to align the nematic phase. Therefore, SmA mixtures with a neighboring nematic phase are especially attractive for applications as birefringent fillers, as the system can be field-aligned in the nematic phase. We also described regular solid crystal birefringent prisms made of YVO$_4$.

We demonstrated that the decoupled rotator-deflector design allows one to assemble multiple beam-deflecting stages into one device with a broad range of deflected directions. As an example, we constructed and tested a four-stage DBD with 16 deflection directions in the angular range of $+56$ to -56 mrad (for normal incidence). We achieved high efficiency of the deflected beams up to 75%.

REFERENCES

[1] McManamon, P. F., Watson, E. A., Dorschner, T. A., & Barnes, L. J. (1993). *Opt. Eng.*, *32*, 2657.
[2] James A. Thomas & Yeshaiahu Fainman (1998). *Appl. Opt.*, *37*, 6196.
[3] Solgaard, O., Sandejas, F. S. A., & Bloom, D. M. (1992). *Opt. Lett.*, *17*, 688.
[4] Fuchs, R., Jerominek, H., Swart, N., Diawara, Y., Lehoux, M., Bilodeau, G., Savard, S., Cayer, F., Rouleau, Y., & Lemire, P. (1998). *Proc. SPIE*, *3513*, 40.
[5] Kim, J.-H., Sun, L., Jang, C.-H., Choi, C.-C., & Chen, R. T. (2003). *Opt. Eng.*, *42*, 620.
[6] Kang, D., Maclennan, J. E., Clark, N. A., Zakhidov, A., & Baughman, R. H. (2001). *Phys. Rev. Lett.*, *86*, 4052.
[7] Mach, P., Wiltzius, P., Megens, M., Weitz, D. A., Lin, K.-H., Lubensky, T. C., & Yodh, A. G. (2002). *Europhys. Lett.*, *58*, 679.
[8] Miniewicz, A., Gniewek, A., & Parka, J. (2002). *Optical Materials*, *21*, 605.
[9] Klaus, W. (2002). *AEU-International Journal of Electronics and Communications*, *56*, 243.
[10] Wu, S.-T., Neubert, M. E., Keast, S. S., Abdallah, D. G., Lee, S. N., Walsh, M. E., & Dorschner, T. A. (2000). *Appl. Phys. Lett.*, *77*, 957.
[11] Golovin, A. B., Shiyanovskii, S. V., & Lavrentovich, O. D. (2003). *Appl. Phys. Lett.*, *83*, 3864.
[12] Charles M. Titus, Philip J. Bos & Oleg D. Lavrentovich (1999). *Proc. SPIE*, 3633, 244.
[13] Titus, C. M. (2000). *Refractive and Diffractive Liquid Crystal Beam Steering Devices*, Dissertation: Chemical Physics Interdisciplinary Program, Kent State University.
[14] McRuer, R., McAdams, L. R., & Goodman, J. W. (1990). *Opt. Lett.*, *15*, 1415.
[15] Lee, T. C., & Zook, J. D. (1968). *IEEE Journal of Quantum El.*, QE-4, 442.
[16] Meyer, H., Riekmann, D., Schmidt, K. P., Schmidt, U. J., Rahlff, M., Schroder, E., & Thust, W. (1972). *Appl. Opt.*, *11*, 1732.
[17] Pepperl, R. (1977). *Opt. Acta*, *24*, 413.
[18] Kulchke, W., Kosanke, K., Max, E., Haberger, M. A., Harris, T. J., & Fleisher, H. (1966). *Appl. Opt.*, *5*, 1657.
[19] Kruger, U., Pepperl, R., & Schmidt, U. J. (1973). *Proceedings of the IEEE*, 61, 992.
[20] Blinov, L. M. & Chigrinov, V. G. (1994). *Electrooptic Effects in Liquid Crystal Materials*, Springer-Verlag: New York, Inc.
[21] de Gennes, P. G. & Prost, J. (1993). *The Physics of Liquid Crystals*, 2nd ed., Clarendon Press: Oxford.
[22] Vertogen, G. & de Jeu, W. H. (1988). *Thermotropic Liquid Crystals*, *Fundamentals*, Springer.
[23] Kleman, M. & Lavrentovich, O. D. (2003). *Soft Matter Physics: An Introduction*. Springer: New York.

[24] Luckhurst, G. R., (2000). *Mol. Cryst. Liq. Cryst.*, *347*, 121.
[25] Luckhurst, G. R., Miyamoto, T., Sugimura, A., & Timimi, B. A. (2000). *Mol. Cryst. Liq. Cryst.*, *347*, 147.
[26] Takanishi, Y., Ouichi, Y., Takezoe, H., & Fukuda, A. (1989). *Jpn. J. Appl. Phys. Lett.*, *28*, L487.
[27] Lavrentovich, O. D., Kleman, M., & Pergamenshchik, V. M. (1994). *J. Phys. II France*, *4*, 377.
[28] Lavrentovich, O. D. & Kleman, M. (1993). *Phys. Rev. E*, *48*, R39.
[29] Maurice Kleman & Oleg D. Lavrentovich (2000). *Phys. Rev. E*, *61*, 1574.
[30] Li, Z. & Lavrentovich, O. D. (1994). *Phys. Rev. Lett.*, *73*, 280.
[31] Jenkins, F. A. & White, H. E. (1976). *Fundamentals of Optics*, 4th ed., McGraw-Hill.
[32] Gooch, C. H. & Tarry, H. A. (1975). *J. Phys. D.: Appl. Phys.*, *8*, 1575.